22

Multifrequency and Multifunction Metamaterial-loaded Printed Antennas

Francisco Javier Herraiz-Martínez, Daniel Segovia-Vargas, Eduardo Ugarte-Muñoz, Luis Enrique García-Muñoz and Vicente González-Posadas
Radiofrequency Group, Carlos III University in Madrid
Spain

1. Introduction

Metamaterials can be broadly defined as electromagnetic structures engineered to achieve exotic or unusual properties (Caloz & Itoh, 2004; Eleftheriades & Balmain, 2005; Engheta & Ziolkowski, 2006; Marqués et al., 2007). Recently these features have been used in microwave and antenna engineering to develop devices with extraordinary properties. For example, microwave devices with extraordinary characteristics such as miniaturization or operation over multiple frequency bands have been developed (Caloz & Itoh, 2004; Eleftheriades & Balmain, 2005; Marqués et al., 2007). The effort in the antenna field has been put on the use of metamaterials for travelling-wave antennas and as substrates and superstrates to enhance the performance of the original antennas (Caloz & Itoh, 2004; Eleftheriades & Balmain, 2005; Engheta & Ziolkowski, 2006). One of the main applications of metamaterial structures in microwave engineering is the development of artificial Left-Handed (LH) Transmission Lines (TLs) (Caloz & Itoh, 2004; Eleftheriades & Balmain, 2005). These TLs are termed as LH because their behaviour is the dual of the conventional or Right-Handed (RH) ones. In the LH TLs, the electric field, magnetic field and propagation vectors form a LH triplet, allowing the propagation of backward-waves, contrary to the conventional case. If we consider a TL as the concatenation of infinite unit cells, the equivalent circuit model of a LH unit cell is a series capacitance and a shunt inductance which is the dual of a RH unit cell (a series inductance and a shunt capacitance) (Caloz & Itoh, 2004).

During the last years, wireless systems have achieved a great popularity and penetration in society. Cellular systems, positioning systems (GPS, Galileo), personal area networks (Bluetooth) and wireless local area networks (WiFi) are good examples. This fact has made that user terminals designed for two or more of these services are very common nowadays. From the antenna engineering point of view, the radiating elements for these terminals require challenging features. The first one is multifrequency, which means that the antennas must work at two or more arbitrary bands simultaneously. Another challenging feature is multifunctionality because in some cases different characteristics, such as polarization or radiation pattern, are required at each working band. Moreover, all these antennas must be small to integrate them into compact handheld devices attractive for the users. Furthermore,

the use of cheap technologies is crucial for mass production. All these requirements cannot be easily achieved with conventional approaches. For that reason, novel technologies such as those based on metamaterial structures are being proposed to fulfil all of these requirements.

The proposed approach is called metamaterial-loaded printed antennas. It is based on conventional printed antennas loaded with a small number of metamaterial particles. Although metamaterial structures are ideally formed by an infinite number of unit cells, a small number of unit cells can be used to achieve devices with enhanced performance for practical purposes. For example, microwave devices such as filters or couplers have been developed with a small number of metamaterial cells (Caloz & Itoh, 2004; Eleftheriades & Balmain, 2005; Marqués et al., 2007). Furthermore, the use of a small number of particles does not increase the complexity and size of the antennas, providing easy design and manufacturing processes and allowing the antennas fit into modern devices. Finally, it is important to note that printed antennas have low profile, light weight, low cost and they are easy to integrate with circuitry and as elements of antenna arrays (Garg et al., 2001; James & Hall, 1989).

In this Chapter two kind of metamaterial-loaded printed antennas are presented. In Section 2 metamaterial-loaded printed dipoles are reviewed (Herraiz-Martínez et al., 2009). Basic theory and several examples are explained, showing the validity of this approach to develop multifrequency printed dipoles. Section 3 is devoted to microstrip patch antennas filled with LH structures (Herraiz-Martínez et al., 2008). A simple TL model of these antennas is used to demonstrate their multifrequency and multifunction features. Two different patch antennas filled with LH structures are studied, manufactured and measured, demonstrating the validity of the approach. Finally, the Chapter is concluded in Section 4.

2. Metamaterial-loaded Printed Dipoles

2.1 LC-loaded Printed Dipoles

The first experiment to show the validity of the metamaterial-loaded printed antennas consists of loading a simple printed wire antenna with LC parallel tanks. These cells have been chosen because most of the elemental metamaterial magnetic cells, such us Split Ring Resonators (SRRs) or spiral resonators, can be modelled as LC parallel tanks, as it was proposed in (Baena et al., 2005).

The reference antenna is an antipodal dipole printed on both sides of a dielectric substrate with height h (Fig. 1). Each half of the antipodal dipole is printed on one side of the substrate. The parameters of the dipole are the length L and the width W of each half. This configuration has been chosen because it avoids the use of a balun to feed the antenna. This is possible because the printed dipole is fed through a paired strips transmission line (Wadell, 1991) with a SMA connector soldered to the end of the line. The outer conductor of the SMA connector is soldered to one strip of the feeding line while the inner conductor is soldered to the other strip of the feeding line. The dimensions of the feeding line are the length L_f and the width W_f.

As an example, a dipole with L = 42.05 mm, W = 2.50 mm, L_f = 27.50 mm and W_f = 1.00 mm is considered. The substrate is the low-cost FR-4 (ε_r = 4.5, tan δ = 0.015 and h = 0.50 mm). These dimensions are chosen to obtain the resonant frequency of the fundamental mode (n = +1) at 1.5 GHz. When working at this mode, the current on the dipole has the $\lambda/2$ sinusoidal

distribution, with minima at the edges of the dipole (open-circuit conditions) and maximum at the centre of the dipole (Fig. 2(a)). This current distribution provides the conventional dipolar-like radiation pattern (Fig. 2(b)).

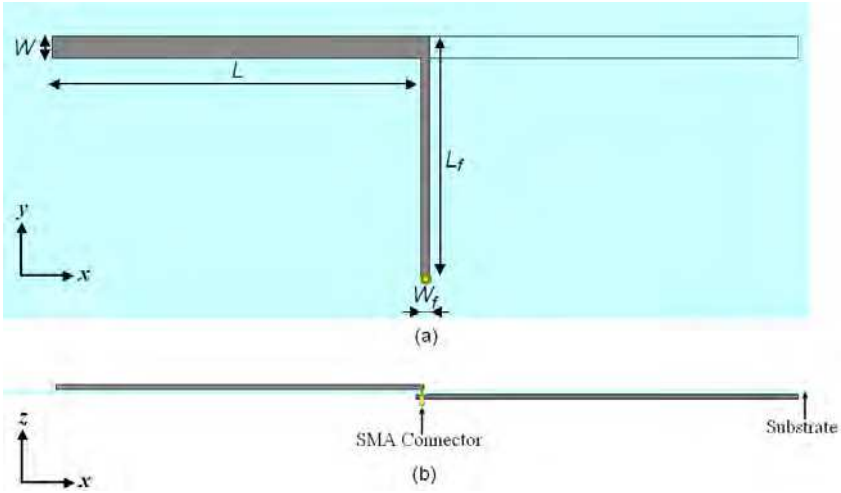

Fig. 1. Sketch of an antipodal printed dipole. (a) Top view. (b) Side view.

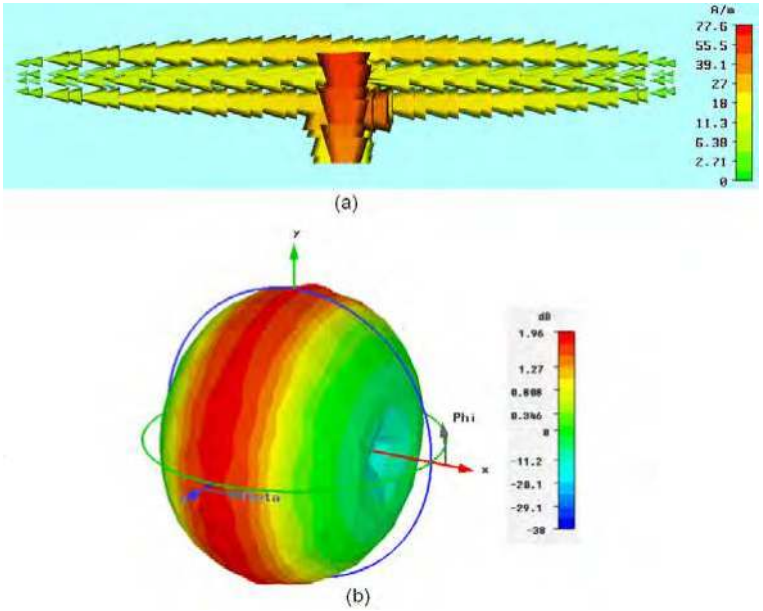

Fig. 2. Fundamental mode of an antipodal printed dipole. (a) Current distribution. (b) Radiation pattern.

To show the validity of the proposed approach, the reference printed dipole is loaded with one LC parallel tank per half, as it is shown in Fig. 3. The values of the LC components are L = 10 nH and C = 0.47 pF. These tanks are placed at a distance d = 35.00 mm from the centre of the dipole. The self-resonant frequency of the LC parallel tanks is computed as

$$f_{LC} = \frac{1}{2\pi\sqrt{LC}} \tag{1}$$

According to this expression the self-resonant frequency of the LC parallel tanks is 2.3 GHz. The proposed LC loaded dipole has been simulated and manufactured. This dipole presents an unusual dual-frequency performance (1.4 GHz and 1.9 GHz), as it is shown in Fig. 4. The first resonance is very close to the fundamental one of the conventional dipole. On the other hand, the second resonance is devoted to the LC parallel tanks, but it has been shifted down towards lower frequencies. It has been observed that when the ratio between the fundamental frequency of the dipole and the self-resonant frequencies of the LC tanks is larger than in this case, the frequency shift of the second resonance is considerably reduced. This is an important feature, because dual-frequency printed dipoles with arbitrary working frequencies can be designed.

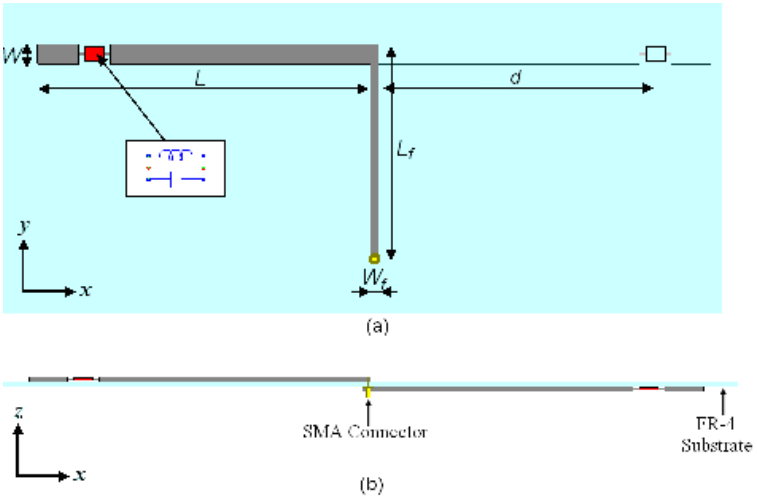

Fig. 3. Sketch of a LC-loaded antipodal printed dipole. (a) Top view. (b) Side view.

The currents on the dipole have a half-wavelength sinusoidal distribution (Fig. 5). At the first frequency they are similar to the unloaded dipole (Fig. 2(a)). On the other hand, the LC tanks impose a hard boundary condition (open-circuit) at the second frequency. This produces that there is almost no current between the tanks and the dipole edges. In this case, the minima are located at the tanks and the maximum is maintained at the feeding point. Both half-wavelength sinusoidal currents provide a dipolar-like radiation pattern (Fig. 6).

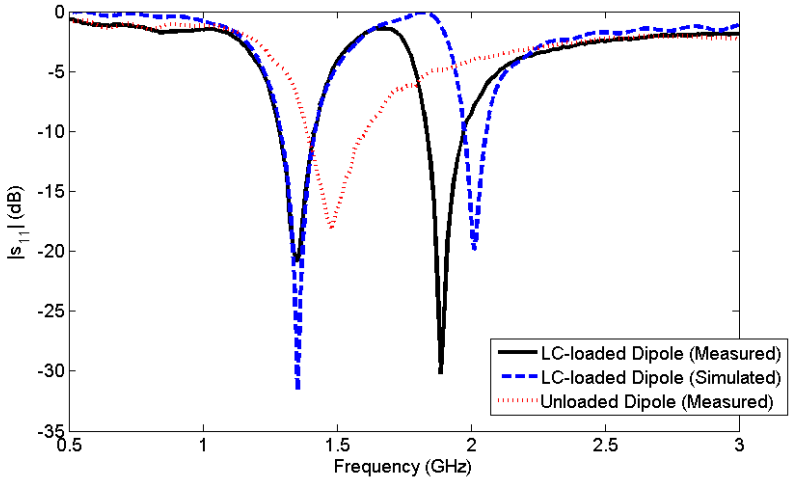

Fig. 4. Measured and simulated reflection coefficient of the LC-loaded dipole. The measured reflection coefficient of the unloaded dipole is also plotted.

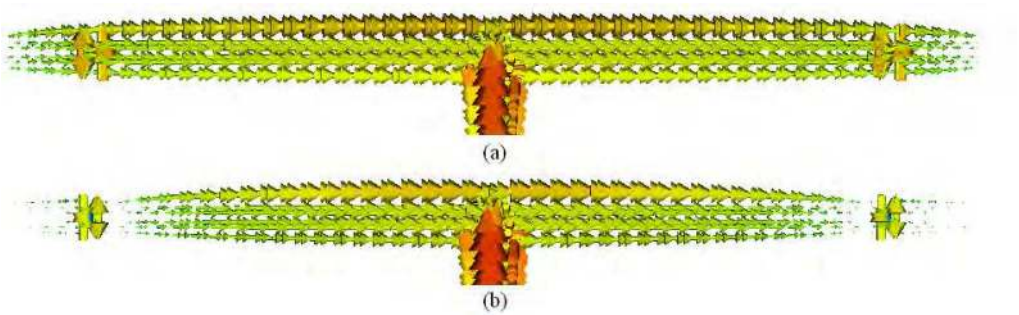

Fig. 5. Simulated currents on the LC-loaded printed dipole. (a) 1.4 GHz. (b) 1.9 GHz.

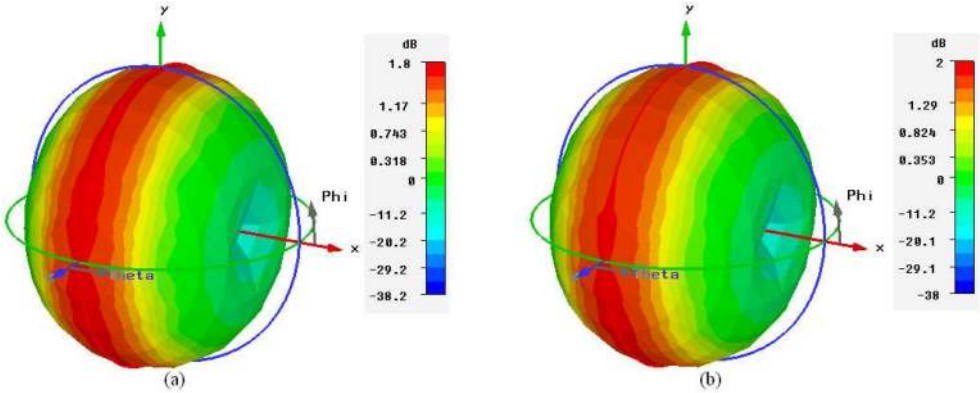

Fig. 6. Radiation patterns of the LC-loaded printed dipole. (a) 1.4 GHz. (b) 1.9 GHz.

2.2 Dual-frequency Metamaterial-loaded Printed Dipoles

The next step consists of loading the antipodal printed dipole with printed metamaterial particles in order to achieve a dual-frequency performance. One metamaterial particle or a set of them are coupled to each half of the dipole. In the example of Fig. 7, four SRRs are printed on the opposite side of each dipole half. This configuration has been chosen because it provides a proper matching within a wide range of ratios between the working frequencies. The SRRs parameters, according to Fig. 7(b), are the external radius R, the width of the strips W_{SRR} and the gap between strips g. The SRRs are placed at a distance c from the dipole centre. The separation between the centers of the SRRs is s. Moreover, other magnetic metamaterial particles can be used to obtain the desired multifrequency performance (spiral resonators, Omega particles …). Regardless of the particular configuration, the metamaterial particles must be located in a way such the magnetic field generated by the currents on the dipole has an important component in the direction perpendicular to the plane of the particles. This is similar to the case of TLs loaded with metamaterial particles (Marqués et al., 2007).

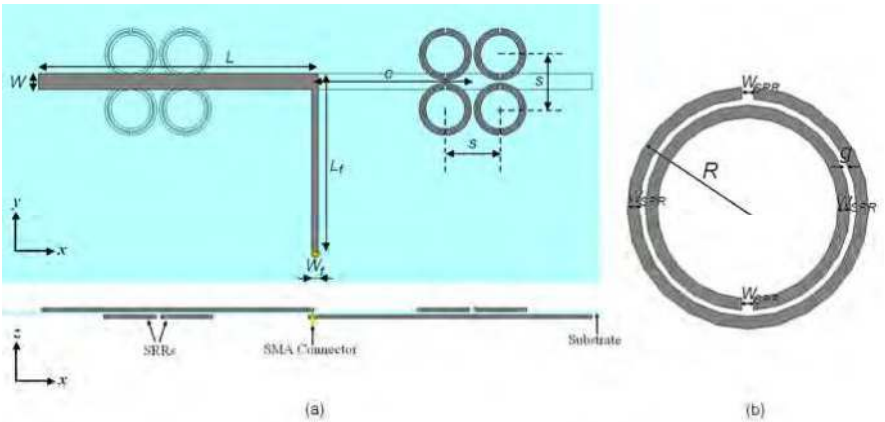

Fig. 7. Sketch of a metamaterial-loaded printed dipole antenna: (a) Top and side views of the antenna with its design parameters. (b) Split Ring Resonator parameters.

A prototype of the proposed SRRs-loaded dipole antenna has been designed. The dimensions of the dipole are kept unchanged: L = 42.05 mm, W = 2.50 mm, L_f = 27.5 mm and W_f = 1.00 mm. The low-cost FR-4 substrate (h = 0.50 mm, ε_r = 4.50 and tan δ = 0.015) has been used. The prototype is loaded with a set of four SRRs per half, placed at a distance c =24.20 mm and the separation s is 8.40 mm. The parameters of the SRRs are the radius R = 4.00 mm, the width W_{SRR} = 0.40 mm and the gap between rings g = 0.20 mm. The theoretical resonant frequency of the unloaded antipodal dipole with these dimensions is 1.5 GHz, as showed in the previous Subsection. According to (Baena et al., 2005) the resonant frequency of the SRRs is 2.55 GHz.

The proposed configuration provides the desired dual-frequency performance. The first frequency (f_1) is close to the fundamental frequency of the dipole (n = +1 mode) while the additional frequency (f_{SRR}) occurs in the vicinity of the SRRs self-resonant frequency. Fig. 8 (obtained with Momentum) shows the current distributions on the proposed dipole at the

two working frequencies. At f_1 (Fig. 8(a)) the current distribution is similar to the one obtained in the conventional $\lambda/2$ dipole (Fig. 2(a)). It can be appreciated that the effect of the SRRs at this frequency is negligible and nearly no current passes along them. This implies that the expected radiation pattern at this frequency is also similar to the reference dipole. In fact, the only modification in the antenna performance is a very slight frequency shift in the resonant frequency towards lower frequencies due to the capacitive parasitic effect of the SRRs. On the other hand, the working principle at f_{SRR} is somewhat different since the resonant frequency is imposed by the SRRs. At this frequency the SRRs are resonating, as can be seen in Fig. 8(b), where the currents through the SRRs are maximum. In this case, the SRRs are not radiating but imposing a hard boundary condition (an open circuit) where they are placed. In this way, the currents in the dipole are nearly zero from this position to the end of the overall dipole. Thus, the effect of the SRRs is similar to the one obtained with the LC parallel tanks in the previous Subsection. This means that the radiating element is formed by the current distribution on the dipole between the SRRs arrangements. It should be noted that this radiating element is a dipole with a length shorter than $\lambda/2$ sustaining a current between the edges where the SRRs are placed. Thus, it is expected that the proposed structure gives a dipolar-like radiation pattern at f_{SRR}. This is an important feature because the proposed dipoles not only present the desired dual-frequency performance but they keep the dipolar-like radiation pattern at both working frequencies.

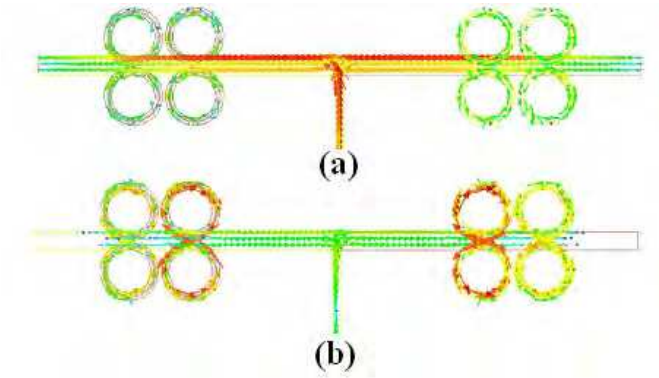

Fig. 8. (a) Currents on the SRRs-loaded dipole at f_1. (b) Currents on the SRRs-loaded dipole at f_{SRR}.

The proposed dual-frequency dipole and the conventional unloaded dipole have been manufactured (Fig. 9(a)). The measured reflection coefficients of both prototypes are shown in Fig 9(b). The reference dipole working frequency is 1.48 GHz, while the proposed SRRs-loaded dipole has the desired dual-frequency performance. The first resonance appears at f_1 = 1.32 GHz. The second working frequency (f_{SRR}) is 2.83 GHz. This frequency is shifted towards higher frequencies due to the overall coupling effects and the tolerances of the substrate and the manufacturing process. The bandwidth at the lower band is around 15% at the -10 dB level for both dipoles. On the other hand, the bandwidth at the additional band (at the -10 dB level) for the proposed dipole is much lower (1.27%). This is due to the high Q factor of the SRRs, what implies a much smaller bandwidth in the resonance imposed by them.

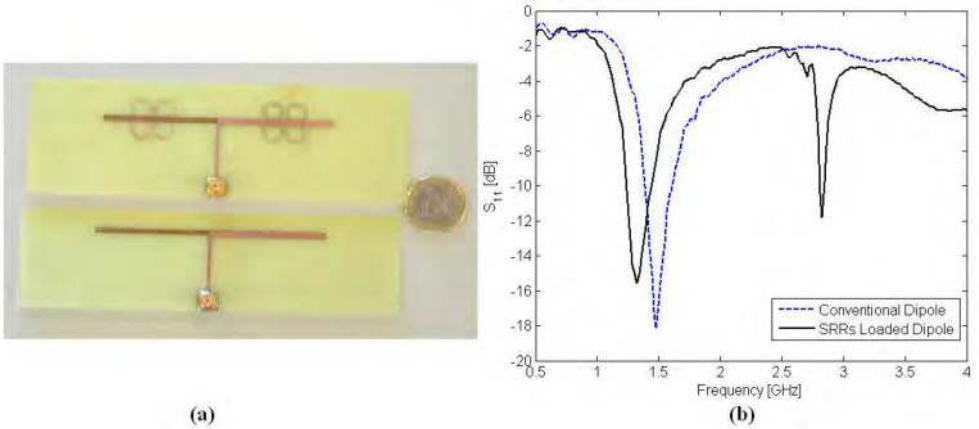

Fig. 9. (a) Picture of the manufactured prototypes: SRRs-loaded antipodal dipole (top) and conventional antipodal dipole (bottom). (b) Measured reflection coefficient of both antennas.

Fig. 10 shows the measured radiation patterns of the proposed dual-frequency dipole at both working frequencies (1.32 GHz and 2.83GHz). Both of them are dipolar and similar to the conventional dipole. A ripple can be noticed especially at the YZ plane because of the presence of a metallic plate, part of the positioner, behind the antenna. The measured gain of the reference dipole is 1.99 dB while the gain of the dual-frequency prototype is 1.81 dB at f_1 and 0.67 dB at f_{SRR}.

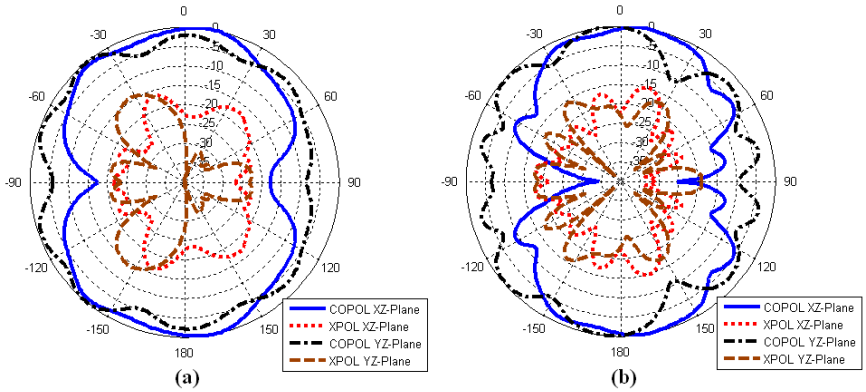

Fig. 10. Measured radiation patterns of the proposed SRR-loaded dipole. (a) f_1 = 1.32 GHz (b) f_{SRR} = 2.83 GHz.

2.3 Multifrequency Metamaterial-loaded Printed Dipoles

The approach to obtain multifrequency printed dipoles (printed dipoles with three or more working frequencies) consists of exciting two or more additional resonances. These additional resonances are obtained with different pairs of metamaterial particles. At least a pair of metamaterial particles must resonate at each desired additional frequency. As an example, a triple-frequency printed dipole is proposed below.

According to Fig. 11, let us consider the case in which $R_2 = R_1 + 0.4$ mm. In this case, the resonant frequencies of the top and bottom pairs of SRRs are separated 0.22 GHz and a triple-frequency antenna can be obtained.

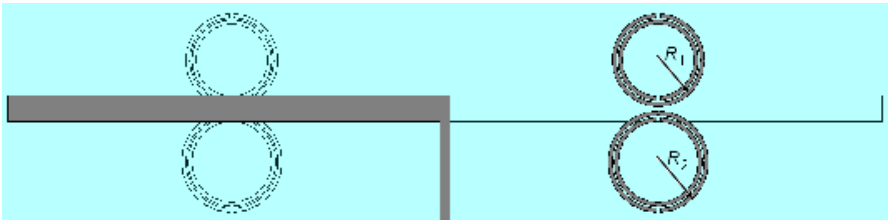

Fig. 11. Sketch of the proposed triple-frequency printed dipole loaded with SRRs.

Fig. 12 shows the simulated (CST Microwave Studio) reflection coefficient of the proposed triple-frequency antenna. The three working frequencies can be easily identified. The $|s_{11}|$ parameters of the dipoles loaded with both SRRs with $R = R_1$ and $R = R_2$ are also plotted. These plots show that the three resonances of the triple-frequency antenna are due to the fundamental frequency of the dipole and the self-resonant frequencies of the SRRs with different dimensions.

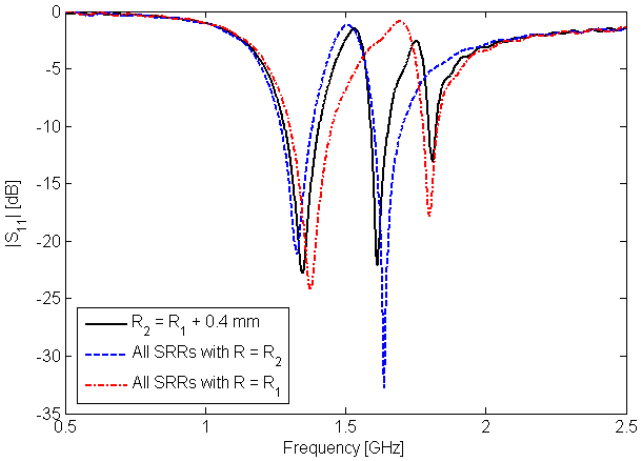

Fig. 12. $|s_{11}|$ parameter of the triple-frequency printed dipole antenna. The same information for the cases in which all the SRRs have the same dimensions is also plotted.

The simulated currents on the antenna at the three working frequencies are shown in Fig. 13. The distributions are similar to the one presented by the dual-frequency dipole (Fig. 8). The SRRs are not resonating at the first working frequency (f_1) and the currents on the dipole are similar to the unloaded dipole (Fig. 2(a)). The SRRs with R_2 are resonating at the second working frequency (f_2). Most of the current on the dipole is between the SRRs and there is almost no current between the SRRs and the edges of the dipole. At the third working frequency (f_3) the distribution is similar to the previous one (f_2) but the SRRs with

R_1 are resonating instead of R_2–SRRs. It is important to note that the radiation pattern is dipolar at the three working frequencies.

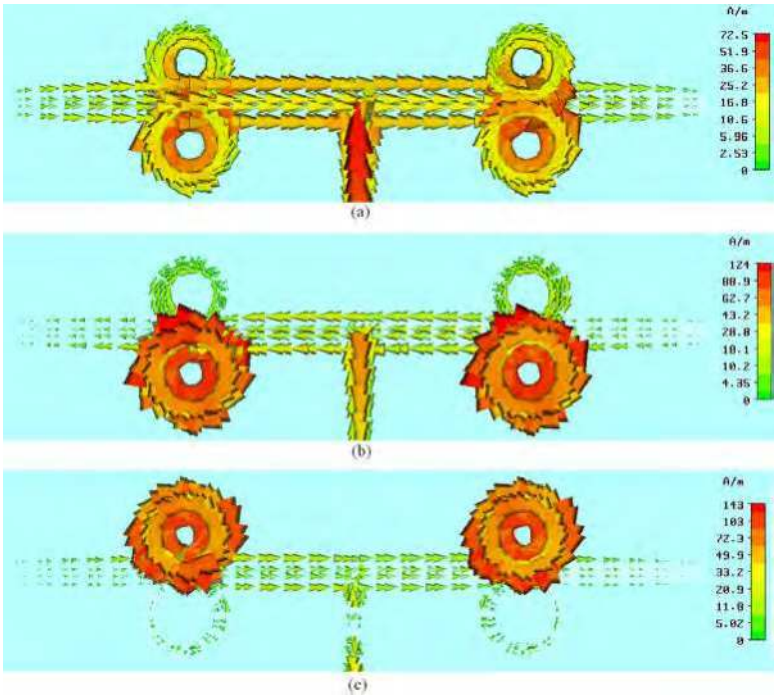

Fig. 13. Currents on the triple-frequency printed dipole loaded with SRRs. (a) f_1 (fundamental frequency of the unloaded dipole). (b) f_2 (resonant frequency of the SRRs with R_2). (c) f_3 (resonant frequency of the SRRs with R_1).

3. Microstrip Patch Antennas Filled with LH Structures

3.1 Simplified Transmission Line Model

A conventional microstrip patch antenna can be modelled as a RH TL. In this case, the resonant condition is given by the following equation:

$$\beta_n L = n\pi \tag{2}$$

where L is the equivalent TL length and n is the resonant index. As the TL has a RH behavior, the propagation constant β is always positive and linear with frequency. This means that all the modes have positive indices (n = +1, +2, +3, ...), all the resonant frequencies are harmonics of the fundamental one ($f_n = n\, f_{+1}$) and all the modes have $n\, \lambda/2$ electric field distribution, which means that all the modes different to the fundamental one have multiple lobes in the radiattion pattern. These characteristics make conventional patch antennas not suitable for multifrequency systems. The first reason is that arbitrary frequencies cannot be achieved because once the fundamental frequency is fixed, the other

frequencies are always multiples of the fundamental one. The second reason is that radiation patterns with multiple lobes are not interesting for most of applications, since that implies a loss of directivity.

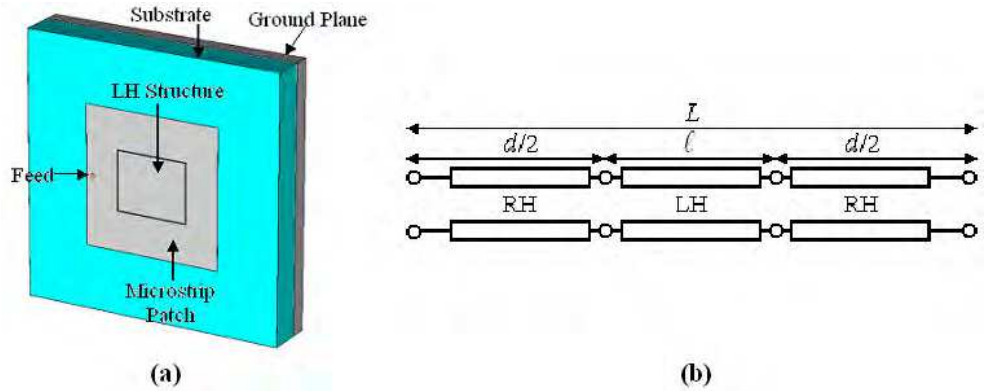

Fig. 14. Microstrip patch filled with LH structures. (a) Sketch of the antenna. (b) Equivalent TL model.

The proposed multifrequency patch antennas are based on a square microstrip patch filled with LH structures (Fig. 14(a)). For simplicity we can consider propagation along one main direction. In this case, the simplest equivalent antenna TL model is composed of a LH section between two RH sections (Fig. 14(b)).
The propagation constant is positive and linear with frequency in the RH sections while it is negative and proportional to $1/f$ in the LH sections. Then, in this case the resonant condition can be written as:

$$\beta_n L = \beta_n^{RH} d + \beta_n^{LH} \ell = k_1 f_n d - \frac{k_2}{f_n} \ell = n\pi \tag{3}$$

where k_1 and k_2 are positive constants; d and ℓ are the equivalent lengths of the RH and LH sections, respectively. In this case, it is possible to obtain modes with negative, zero or positive indices, contrary to the conventional case. Specifically, for a LH section composed of M unit cells, n takes values:

$$n = -M+1, -M+2, \ldots, -1, 0, +1, +2, \ldots \tag{4}$$

In particular if $M \geq 2$, two interesting modes are achieved below the mode equivalent to the fundamental one of the conventional patch antenna:
The first one is the $n = -1$ mode when the condition $\beta\ell = -\pi$ is satisfied. This mode has a half-wavelength electric field distribution similar to the fundamental mode of a conventional patch antenna. Thus, a patch-like radiation pattern is achieved at this mode.
The second one is the $n = 0$ mode when the condition $\beta\ell = 0$ is achieved. This mode has a uniform electric field distribution in amplitude and phase inside the patch antenna, which gives a monopolar radiation pattern (null at broadside). This type of radiation pattern cannot be achieved with conventional patches and only is present in short-circuited patch

antennas (González-Posadas et al., 2006). The possibility of using this mode provides a degree of multifunctionality due to the fact that radiation pattern diversity can be achieved with these antennas.
Moreover, the conventional (RH) modes ($n \geq +1$) are also present in the proposed antennas.
It is important to note that the resonant frequencies are not forced to follow a harmonic ratio in this case. This is possible thanks to the non-linear behaviour introduced by the LH section.
In conclusion, two interesting kinds of multifrequency patch antennas can be developed with this approach. The first one is a dual-band patch antenna with patch-like radiation pattern at both bands by using the $n = \pm 1$ modes simultaneously. Moreover, when the $n = 0$ mode is also excited, a triple-frequency and dual-mode patch antenna is obtained. Examples of both antennas are presented below.

3.2 Triple-frequency and Dual-mode Microstrip Patch Antenna

The proposed antenna is shown in Fig. 15(a) where the patch dimensions (L x W) are 42 mm x 42 mm. The substrate is polypropylene (PP) with $\varepsilon_r = 2.2$ and $h = 10$ mm. The LH structure is implemented by using mushroom-type cells. These cells are based on microstrip patches grounded with vias and separation gaps between the cells. The vias provides the shunt inductances and the gaps the series capacitances of the LH section (Sanada et al., 2004). In particular, in this antenna the LH structure is based on a 2 x 1 mushroom-type cell array configuration and the dimensions of the mushrooms (L_m x W_m) are 10.6 mm x 17.8 mm. The diameter of the vias (d) is 0.7 mm, the gap between the two mushrooms (g_1) is 0.40 mm and the separation gap between the microstrip patch and the LH structure (g_2) is 0.20 mm. The antenna is fed through a coaxial probe placed 14 mm away from the centre. The dimensions of the ground plane are 80 mm x 80 mm. These dimensions were chosen to obtain the resonant frequencies at 1 GHz (GSM-900 band) for the $n = -1$ mode, 1.5 GHz (positioning systems) for the $n = 0$ mode and 2.2 GHz (UMTS) for the $n = +1$ mode.

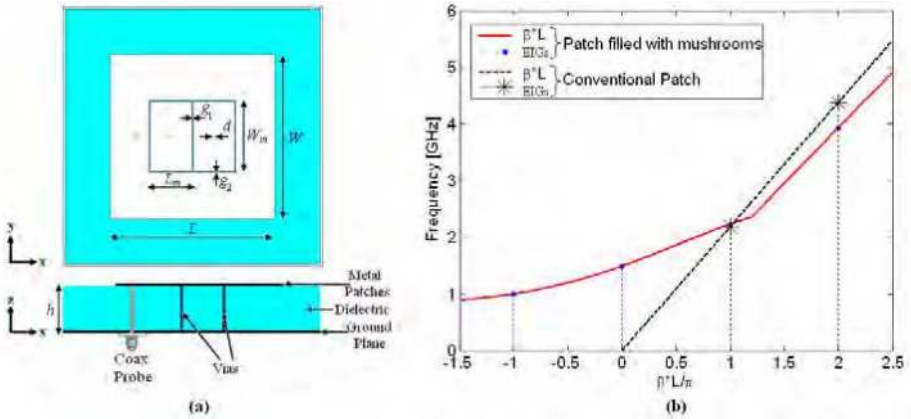

Fig. 15. Triple-frequency and dual-mode antenna based on a microstrip patch filled with LH cells. (a) Sketch of the antenna. (b) Electrical length (βL) and eigenfrequencies (EIGs) of the resonant modes of the proposed antenna (solid red line). The same information for the conventional patch antenna is also plotted in the dashed line.

Fig. 15(b) shows the electrical length of the proposed antenna versus frequency and the eigenfrequencies of the modes obtained through full-wave simulation. The same information for the conventional square patch antenna is also plotted. The electrical lengths have been computed by interpolating the discrete values of the eigenfrequencies. The linear ratio between the electrical length and frequency for the conventional patch antenna can be appreciated. On the other hand, the patch partially filled with the mushroom structures has the same relation for the modes with positive indices, but it has a LH behaviour at lower frequencies. This LH relation has been computed with the eigenfrequencies method (Herraiz-Martínez et al., 2007). The chart shows that for the index n = +1, the working frequency is very close to the fundamental frequency of the conventional patch (but not equal due to the residual LH effect of the metamaterial structure). As a first approximation for general design, the patch length is chosen to obtain the n = +1 frequency as the fundamental mode of the patch without mushrooms. On the other hand, the frequencies of the lower modes ($n \leq 0$) strongly depend on the mushroom structure selection. Large mushrooms lead to higher separation between the working frequencies and thus, higher slope in the LH region, while smaller mushrooms provide closer resonances and smaller slopes in the LH region of the electrical length chart. Then, the higher frequency (n = +1 mode) will mainly depend on the patch length (L), while the resonant frequencies of the other modes can be fixed by choosing the adequate mushroom parameters (basically L_m, W_m and the gaps, because the effect of the vias diameter d can be neglected). A detailed parametric study has been carried out in (Herraiz-Martínez et al., 2008).

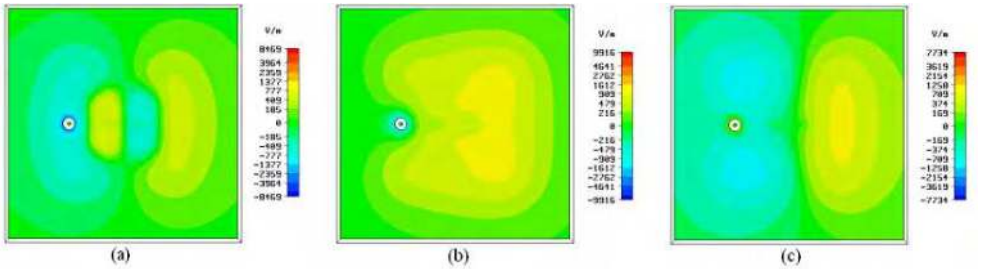

Fig. 16. Electric field distributions of the proposed antenna: (a) n = –1 mode (f_{-1} = 1.06 GHz), (b) n = 0 mode (f_0 = 1.45 GHz), (c) n = +1 mode (f_{+1} = 2.16 GHz)

The electric field distributions (CST Microwave Studio) for the modes with n = –1, n = 0 and n = +1 indices are shown in Fig. 16. The electric field distributions for the n = ±1 modes have half-wavelength electrical length (maximum in amplitude and 180º phase shift at the edges and null at the centre of the patch), similarly to the fundamental mode of a conventional patch antenna. A local 180º phase shift is observed inside the mushroom structure at f_{-1}, but this singularity does not affect the radiation behavior, as it will be shown in the radiation pattern of the experimental results. On the other hand, there is no local phase shift at f_{+1}. Lastly, the electric field distribution is almost uniform in phase and amplitude at f_0, as was predicted.

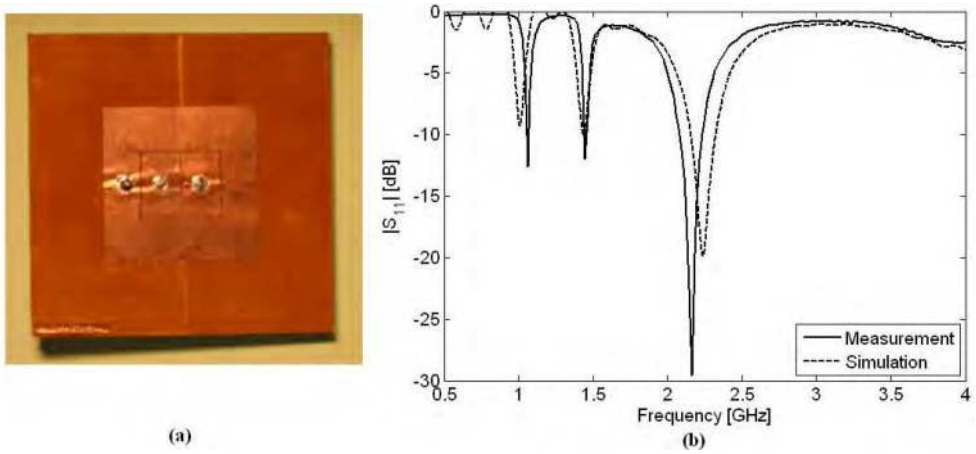

Fig. 17. (a) Picture of the triple-frequency and dual-mode patch antenna. (b) Simulated and measured reflection coefficient of the proposed antenna.

A prototype of this patch antenna has been manufactured (Fig. 17(a)). Fig. 17(b) shows the measured reflection coefficient. The return losses are –12.62 dB at f_{-1}= 1.06 GHz, –12.01 dB at f_0 = 1.45 GHz and –9.59 dB at f_{+1} = 2.16 GHz. The ratio between the resonant frequencies of the first and second modes is 1.37 and the ratio between the two dipolar modes is 2.04. The ratio between these modes can be arbitrarily chosen and depends on the patch and mushrooms dimensions, as explained before. The patch length is $\lambda_0/6.74$ at f_{-1}, $\lambda_0/4.92$ at f_0 and $\lambda_0/3.31$ at f_{+1}. It can be seen that a multifrequency antenna with different radiation modes has been obtained. Moreover, the length is strongly reduced with respect to the conventional $\lambda/2$ patch antennas at the additional frequencies.

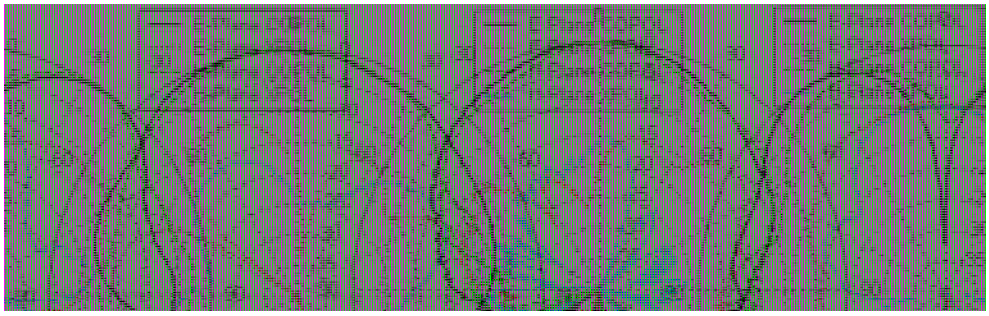

Fig. 18. Measured radiation patterns of the triple-frequency and dual-mode patch antenna. (a) n = –1 mode (1.06 GHz). (b) n = 0 mode (1.45 GHz). (c) n = +1 mode (2.16 GHz).

Finally, Fig. 18 shows the measured radiation patterns of the E-plane (x-z plane) and H-plane (y-z plane) and their corresponding cross-polar components. For the n = –1 mode (1.06 GHz) a patch-like radiation pattern can be seen in Fig. 18(a). The radiation pattern of the n = 0 mode (1.45 GHz) is monopolar as it can be seen in Fig. 18(b). A null in the broadside direction is appreciated. The depth of this null is 16 dB for the E-plane radiation pattern and

15 dB for the H-plane pattern. Two comments must be made concerning the n = 0 mode. First, the maximum of the radiation pattern that would be in the endfire direction is somewhat reduced due to the effect of the finite ground plane. Secondly, the n = 0 mode is excited in a weaker way than the n = 0 mode in a short circuited patch antenna (González-Posadas et al., 2006). This can be seen because of the higher level of the cross-polar component with respect to the short-circuited patch. The broadside radiation pattern is also achieved for the n = +1 mode (2.16 GHz, Fig. 18(c)). The measured gain of the antenna is –3 dB at f_{-1}, 1 dB at f_0 and 6.5 dB at f_{+1}. The gain of the additional modes (n = –1, 0) is reduced with respect to conventional patches because the electrical length of the patch antenna is also smaller due to the miniaturization achieved.

3.3 Dual-frequency Microstrip Patch Antenna

The proposed antenna is designed to work with similar radiation characteristics at 1.8 GHz (DCS band) and 2.2 GHz (UMTS band). Then, the first working frequency is obtained for the n = −1 mode while the second one is obtained for the n = +1 mode. Therefore, a patch-like radiation pattern is achieved at the two frequencies. The monopolar mode (n = 0) is not to be excited in this case. It has been seen that when the vias are aligned with respect to the probe, the ratio between the different working frequencies is higher and the n = 0 mode is excited. On the other hand, when the vias are not located in line with the probe, the frequency ratio between the patch-like modes (n = ±1) is reduced and the monopolar mode (n = 0) is weakly excited. For that reason, the number of cells in the y-direction has been doubled (resulting in a 2 x 2 LH structure instead of a 2 x 1) so the vias are not aligned with the feeding probe.

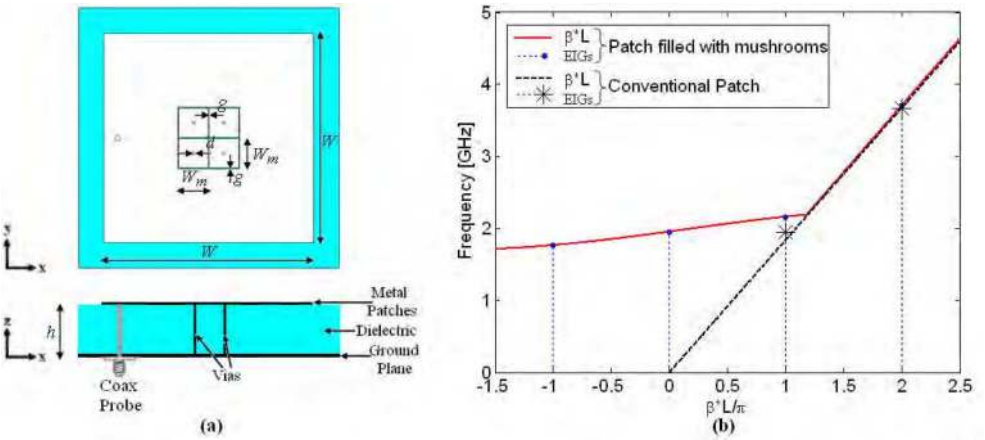

Fig. 19. Dual-frequency antenna based on a microstrip patch filled with LH cells. (a) Sketch of the antenna. (b) Electrical length (β L) and eigenfrequencies (EIGs) of the resonant modes of the proposed antenna (solid red line). The same information for the conventional patch antenna is also plotted in the dashed line.

Thus, the proposed design is shown in Fig. 19(a). It consists of a 48.2 mm square patch (W = 48.2 mm) partially filled with a 2 x 2 mushroom arrangement. The substrate is Polypropylene (PP) with ε_r = 2.2 and h = 8 mm. The mushrooms are squares of W_m = 6.8

mm, the vias diameter (d) is 0.70 mm and the separation gaps (g) are 0.2 mm. The patch is fed through a coaxial probe placed at 21 mm from the centre.
The modes of the proposed patch and its electrical length computed as in the previous case (Section 3.2) are plotted in Fig. 19(b). Once again, the antenna has a LH behavior at low frequencies and the conventional effect at higher frequencies. In this case, the slope in the LH region is lower than in the previous antenna (Fig. 15(b)) to produce the desired reduction in the frequency ratio between the patch-like modes.

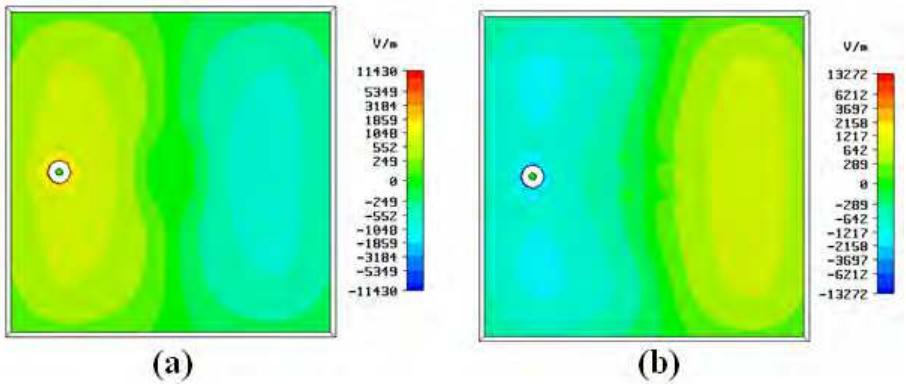

Fig. 20. Electric field distributions for the proposed antenna: (a) n = –1 mode (f_{-1} = 1.81 GHz), (b) n = +1 mode (f_{+1} = 2.20 GHz)

Fig. 20 shows the electric field distributions (CST Microwave Studio) at the two working modes (n = ±1). Similar half-wavelength electric fields distributions are obtained at the two frequencies.

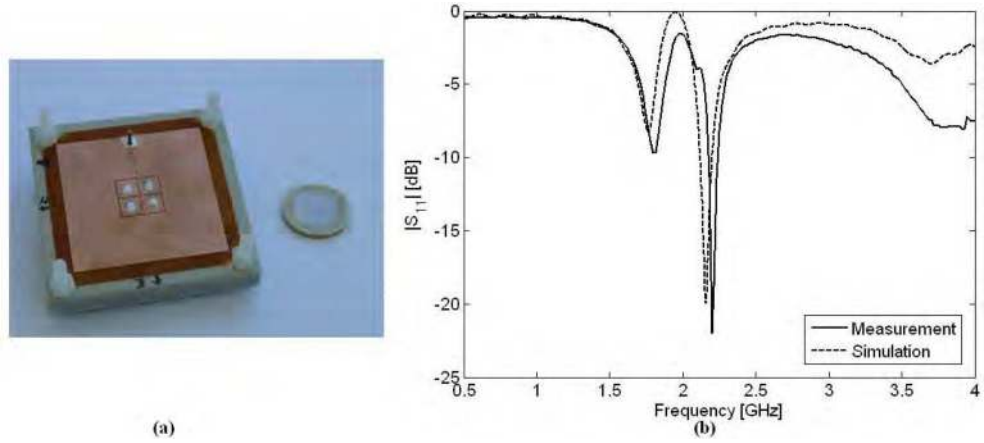

Fig. 21. (a) Picture of the dual-frequency patch antenna. (b) Simulated and measured reflection coefficient of the proposed antenna.

Fig. 21(a) shows a picture of the dual-frequency antenna. The simulated and measured return losses are shown in Fig. 21(b). The measured return losses are −9.83 dB at f_{-1} = 1.81 GHz and −22.03 dB at f_{+1} = 2.20 GHz. The ratio between these two frequencies is 1.21, which is very difficult to achieve to achieve with another single-layer approach. In addition, a reduction factor in comparison with the conventional patch antenna has also been achieved for the n = −1 mode. In this case the patch length is $\lambda_0/3.44$ at f_{-1} and $\lambda_0/2.83$ at f_{+1}.

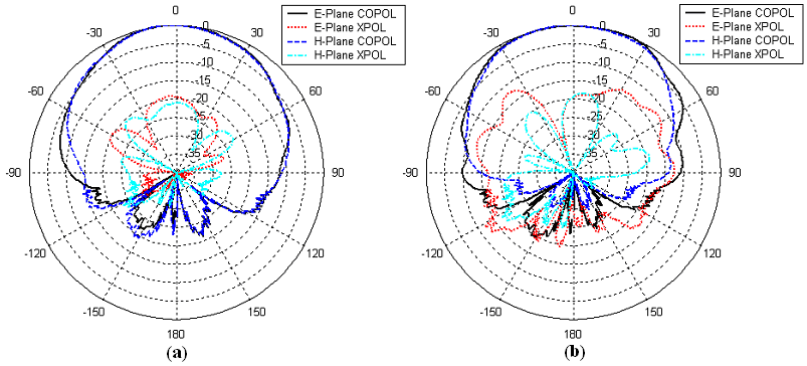

Fig. 22. Measured radiation patterns of the dual-frequency patch antenna. (a) n = −1 mode (1.81 GHz). (b) n = +1 mode (2.20 GHz).

The measured radiation patterns are shown in Fig. 22. The desired patch-like radiation pattern is obtained at both working frequencies. The XPOL component in the broadside direction is approximately −20 dB at both working frequencies. The measured gain of the antenna is 4.5 dB at the first working frequency and 6.8 dB at the second one.

4. Conclusion

Nowadays there is a huge demand on antennas with challenging requirements such us multifrequency, multifunctionality, miniaturization and low cost. All of these features cannot be achieved with conventional approaches. For that reason, novel approaches based on new technologies such us metamaterial structures are being developed. One of these approaches is the one presented in this Chapter: metamaterial-loaded printed antennas. In the present Chapter, it has been demonstrated the validity of this approach to develop antennas with such features. In particular, two kind of metamaterial-loaded antennas have been proposed. The first one is metamaterial-loaded printed dipoles and the second one is microstrip patch antennas filled with LH structures.

Regarding the first kind of antennas, three steps have been followed: initially the dipoles have been loaded with LC parallel tanks achieving dual-frequency performance. After that, the same characteristic has been achieved by loading the dipoles with metamaterial particles. Finally, metamaterials with different resonant frequencies have been used to achieve more than two working frequencies simultaneously. Several prototypes have been designed and manufactured showing good results.

For the microstrip patch antenna filled with LH structures, a simplified TL model has been presented to explain their multifrequency and multifunction behaviour. Moreover, two

practical implementations have been proposed: a triple-frequency and dual-mode patch antenna and a dual-frequency patch antenna with reduced ratio between the working frequencies. All the results have been validated experimentally.

5. References

Baena, J. D.; Bonache, J.; Martín, F.; Marqués, R.; Falcone, F.; Lopetegui, T.; G. Laso, M. A.; García, J., Gil, I. & Sorolla, M. (2005). Equivalent circuit models for split ring resonators and complementary split ring resonators coupled to planar transmission lines. IEEE Transactions on Microwave Theory and Techniques, Vol. 53, No. 4, (April 2005), pp. 1451-1461, ISSN: 0018-9480

Caloz, C. & Itoh, T. (2004). Electromagnetic Metamaterials: Transmission Line Theory and Microwave Applications, Wiley-IEEE Press, ISBN: 0-471-669-857, New York

Eleftheriades, G. V. & Balmain, K. G. (2005). Negative-Refraction Metamaterials: fundamental principles and applications, Wiley-IEEE Press, ISBN: 0-471-601-462, New York

Engheta, N. & Ziolkowski, R. W. (2006). Metamaterials: Physics and Engineering Explorations, Wiley-IEEE Press, ISBN: 0-471-761-028, New York

Garg, R.; Bhartia, P.; Bahl, I.. & Ittipiboon, A. (2001). Microstrip Antenna Design Handbook, Artech House, ISBN: 0-89006-513-6, Norwood

González-Posadas, V.; Segovia-Vargas, D.; Rajo-Iglesias, E.; Vázquez-Roy, J. L. & Martín-Pascual, C. (2006). Approximate Analysis of Short Circuited Ring Patch Antenna Working at TM01 Mode. IEEE Transactions on Antennas and Propagation, Vol. 54, No. 6, (June 2006), pp. 1875-1879, ISSN: 0018-926X

Herraiz-Martínez, F. J.; González-Posadas, V.; Iñigo-Villacorta, F. & Segovia-Vargas, D. (2007). Low-cost Approach based on an Eigenfrequency Method to obtain the Dispersion Diagram in CRLH Structures. IEEE Microwave and Wireless Components Letters, Vol. 17, No.1, (January 2007), pp. 13-15, ISSN: 1531-1309

Herraiz-Martínez, F. J.; García-Muñoz, L. E.; González-Posadas, V. & Segovia-Vargas, D. (2008). Multi-frequency and dual mode patch antennas partially filled with Left-Handed structures. IEEE Transactions on Antennas and Propagation, Vol. 58, No. 8, Part 2, (August 2008), pp. 2527-2539, ISSN: 0018-926X

Herraiz-Martínez, F. J.; García-Muñoz, L. E.; González-Overjero, D.; González-Posadas V. & Segovia-Vargas, D. (2009). Dual-frequency printed dipole loaded with Split Ring Resonators. IEEE Antennas and Wireless Propagation Letters, Vol. 8, (2009), pp. 137-140, ISSN: 1536-1225

James, J. R. & Hall, P. S. (1989). Handbook of Microstrip Antennas, Peter Peregrinus, ISBN: 0-86341-150-9, London

Marqués, R.; Martín, F. & Sorolla, M. (2007). Metamaterials with Negative Parameters, John Wiley & Sons, ISBN: 978-0-471-74582-2, Hoboken, NJ

Sanada, A.; Caloz, C. & Itoh, T. (2004). Planar Distributed Structures with Negative Refractive Index. IEEE Transactions on Microwave Theroy and Techniques, Vol. 52, No. 4, (April 2004), pp. 1252-1263, ISSN: 0018-9480

Wadell, B.C. (1991). Transmission Line Design Handbook, Artech House, ISBN: 0-89006-436-9, Norwood, MA

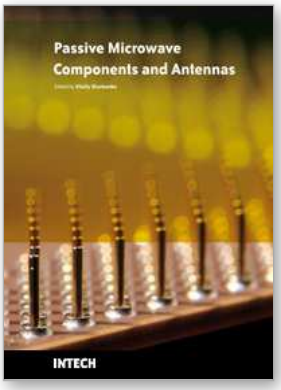

Passive Microwave Components and Antennas

Edited by Vitaliy Zhurbenko

ISBN 978-953-307-083-4
Hard cover, 556 pages
Publisher InTech
Published online 01, April, 2010
Published in print edition April, 2010

Modelling and computations in electromagnetics is a quite fast-growing research area. The recent interest in this field is caused by the increased demand for designing complex microwave components, modeling electromagnetic materials, and rapid increase in computational power for calculation of complex electromagnetic problems. The first part of this book is devoted to the advances in the analysis techniques such as method of moments, finite-difference time- domain method, boundary perturbation theory, Fourier analysis, mode-matching method, and analysis based on circuit theory. These techniques are considered with regard to several challenging technological applications such as those related to electrically large devices, scattering in layered structures, photonic crystals, and artificial materials. The second part of the book deals with waveguides, transmission lines and transitions. This includes microstrip lines (MSL), slot waveguides, substrate integrated waveguides (SIW), vertical transmission lines in multilayer media as well as MSL to SIW and MSL to slot line transitions.

InTech Europe
University Campus STeP Ri
Slavka Krautzeka 83/A
51000 Rijeka, Croatia
Phone: +385 (51) 770 447
Fax: +385 (51) 686 166
www.intechopen.com

InTech China
Unit 405, Office Block, Hotel Equatorial Shanghai
No.65, Yan An Road (West), Shanghai, 200040, China
中国上海市延安西路65号上海国际贵都大饭店办公楼405单元
Phone: +86-21-62489820
Fax: +86-21-62489821